

Cross-correlations of diffuse noise in an ocean environment using eigenvalue based statistical inference

Ravishankar Menon,^{a)} Peter Gerstoft, and William S. Hodgkiss
*Marine Physical Laboratory, Scripps Institution of Oceanography, University of California San Diego,
9500 Gilman Drive, La Jolla, California 92093-0238*

(Received 8 May 2012; revised 23 August 2012; accepted 10 September 2012)

Cross-correlations of diffuse noise fields can be used to extract environmental information. The influence of directional sources (usually ships) often results in a bias of the travel time estimates obtained from the cross-correlations. Using an array of sensors, insights from random matrix theory on the behavior of the eigenvalues of the sample covariance matrix (SCM) in an isotropic noise field are used to isolate the diffuse noise component from the directional sources. A sequential hypothesis testing of the eigenvalues of the SCM reveals eigenvalues dominated by loud sources that are statistical outliers for the assumed diffuse noise model. Travel times obtained from cross-correlations using only the diffuse noise component (i.e., by discarding or attenuating the outliers) converge to the predicted travel times based on the known array sensor spacing and measured sound speed at the site and are stable temporally (i.e., unbiased estimates). Data from the Shallow Water 2006 experiment demonstrates the effectiveness of this approach and that the signal-to-noise ratio builds up as the square root of time, as predicted by theory. © 2012 Acoustical Society of America. [http://dx.doi.org/10.1121/1.4754558]

PACS number(s): 43.60.Fg, 43.60.Cg, 43.50.Rq [ZHM]

Pages: 3213–3224

I. INTRODUCTION

Over the past decade, there has been significant interest in retrieving information from diffuse, multiply scattered, and refracted waves in an environment. It was demonstrated, both theoretically and experimentally,^{1–5} that temporal cross-correlations of a diffuse noise field recorded on a pair of receivers yielded the Green's function between those two points. It also is possible to image remote areas of the ocean^{6–10} and the interior of the earth^{11–13} using diffuse noise fields, as opposed to using controlled active sources which are both expensive and limited in resolution.

The ocean noise field has two primary components—a rich and varied background diffuse noise field due to wind, breaking waves, biological activities, distant shipping, and a highly directional (and often stronger) noise field due to ships and other similar anthropogenic activities in the vicinity of the observing sensors. Depending on whether one wishes to monitor the changes in the environment, or the movement of the sources, the two components of the noise field can either be beneficial or a deterrent. A challenge in using ocean noise is separating these two components reliably.

For an N element linear hydrophone array, the sample covariance matrix (SCM) is formed in the frequency domain from M snapshot vectors (i.e., the Fourier coefficients of the data observation vector at a frequency f), $\mathbf{x}_m(f)$, $m = 1, \dots, M$ as

$$\hat{\mathbf{R}}(f) = \frac{1}{M} \sum_{m=1}^M \mathbf{x}_m(f) \mathbf{x}_m^H(f), \quad (1)$$

and its eigendecomposition gives the eigenvalues $\hat{\lambda}_1(f) \geq \dots \geq \hat{\lambda}_N(f)$ and eigenvectors $\hat{\mathbf{v}}_1(f), \dots, \hat{\mathbf{v}}_N(f)$. The time domain cross-correlation of the data from the i th and j th hydrophones across the entire bandwidth is obtained as

$$\hat{C}_{ij}(t) = \mathcal{F}^{-1}[\hat{\mathbf{R}}_{ij}(f)], \quad (2)$$

where t denotes the correlation time, and \mathcal{F}^{-1} denotes an inverse Fourier transform (henceforth, the dependence on f is dropped unless necessary).

When the noise field is diffuse, the cross-correlation can be used as a proxy for the Green's function of the environment (which is unknown) shaped by the spectrum of the noise field. Hence, the location of the peak of the cross-correlation gives the travel time which typically corresponds to the direct path propagation between the hydrophones.

It was shown experimentally⁶ that in order to obtain stable travel times for a ship dominated noise field, the cross-correlations must be averaged over ship tracks which pass through the end-fire region of a pair of hydrophones. Performing the cross-correlations over much shorter time periods introduces biased travel times because the directional nature of the noise field results in travel times that generally are less than that for the direct path between the hydrophones.^{14,15} This results in requiring long observation times to obtain stable estimates of the travel times.

In this article, the focus is on obtaining stable cross-correlations from an array of sensors without interference from loud sources, by effectively discarding or attenuating the contributions from the directional noise field (Sec. IV). This is achieved by drawing on insights from random matrix theory (RMT) on the behavior of the eigenvalues (Sec. II) of the SCM, which then is used in a statistical hypothesis testing framework (Sec. III).

^{a)}Author to whom correspondence should be addressed. Electronic mail: rmenon@ucsd.edu

RMT, which has its roots in nuclear physics,¹⁶ is a mathematical tool that allows one to study the eigenvalue densities of random matrices in the asymptotic limit as the matrix size increases. It has diverse applications in a wide variety of fields such as statistics,^{17,18} signal processing,^{19–25} ocean acoustics,^{23,26–29} information theory and wireless communications,^{30,31} elastodynamics,³² wave propagation, and scattering in random media.^{33–35}

Recently, the asymptotic eigenvalue densities of the SCM for a three-dimensional (3D) isotropic noise field were derived using RMT.²³ Here, we assume the diffuse background noise field in an ocean environment to be isotropic and use these results to distinguish the eigenvalues due to loud, directional sources (e.g., nearby ships) in the data from those of the background noise using hypothesis testing. Prior related works include model order estimation for signals in white noise using RMT combined with an information theoretic criterion²¹ and eigenvalue based sequential hypothesis testing in white and colored noise.^{17,22} The contribution of this article is in adapting the sequential testing to diffuse ocean noise fields, especially when the SCM inherently is rank deficient (see Sec. II B), and its application in noise processing.

The isotropic noise model is primarily chosen because the known analytical results²³ can be readily related to features observed in data (see Sec. IV). In practice, any reasonable physical noise model can be used (see Sec. V for a brief discussion) and the advantage of using simple analytical noise models is that one can process the data without having to know anything about the environment (e.g., water depth, seafloor characteristics, etc.).

A. Notations and definitions

- (1) The term *eigenvalue density* (probability density of the eigenvalues) is often used, and is defined for any $N \times N$ Hermitian matrix \mathbf{A} with eigenvalues $\{a_1, \dots, a_N\}$ as

$$p_{\mathbf{A}}(x) = \frac{1}{N} \sum_{n=1}^N \delta(x - a_n) = \frac{d}{dx} P_{\mathbf{A}}(x), \quad (3)$$

where $P_{\mathbf{A}}(x)$ is the empirical cumulative distribution (ECD) of the eigenvalues, defined as

$$P_{\mathbf{A}}(x) = \frac{\#\{a_n \leq x\}}{N}, \quad (4)$$

and $\#$ denotes the cardinality of the set.

- (2) As $N \rightarrow \infty$, the ECD of the eigenvalues, $P_{\mathbf{A}}(x)$ converges almost surely to a well-defined distribution $P(x)$ ³⁶ and the corresponding density function, $p(x)$ is referred to as the *asymptotic eigenvalue density*.
- (3) The dimensions of any covariance matrix (CM) \mathbf{A} , unless made explicit, are taken to be $N \times N$. \mathbf{A}_{∞} denotes $\lim_{N \rightarrow \infty} \mathbf{A}_N$. Similarly, any SCM $\hat{\mathbf{A}}$, unless otherwise stated, is taken to be such that $M \hat{\mathbf{A}} \sim \mathcal{W}(\mathbf{A}, M)$, i.e., $M \hat{\mathbf{A}}$ is complex Wishart distributed with M degrees of freedom and true CM \mathbf{A} . $\hat{\mathbf{A}}_{\infty}$ denotes $\lim_{N, M \rightarrow \infty} \hat{\mathbf{A}}_N$, with $N/M = \nu$.
- (4) The term *loud source* is used generically to mean discrete sources or interferers in the environment, which in general

are louder than the diffuse background noise field and possibly could bias the cross-correlations because of their spatial compactness (also see Sec. III A 1).

II. BACKGROUND

A. Statistical model for the SCM

The m th snapshot vector, \mathbf{x}_m , is modeled as

$$\mathbf{x}_m = \mathbf{s}_m + \mathbf{n}_m, \quad (5)$$

where $\mathbf{s}_m \sim \mathcal{CN}(0, \mathbf{S})$ is a circular complex normal distributed directional noise vector from loud sources in the environment with a CM \mathbf{S} and $\mathbf{n}_m \sim \mathcal{CN}(0, \mathbf{\Sigma})$ is a Gaussian diffuse noise vector with a CM $\mathbf{\Sigma}$. From the independence of \mathbf{s}_m and \mathbf{n}_m , the true CM of \mathbf{x}_m is then

$$\mathbf{R} = \mathbf{S} + \mathbf{\Sigma}, \quad (6)$$

and the SCM in Eq. (1) is complex Wishart distributed with M degrees of freedom and true CM \mathbf{R} , i.e., $M\hat{\mathbf{R}} \sim \mathcal{W}(\mathbf{R}, M)$.

For the purposes of this paper, to model the effect of a few loud sources, we assume that the rank of \mathbf{S} , say K , is small compared to the rank of $\mathbf{\Sigma}$, i.e.,

$$K = \text{rank}(\mathbf{S}) \ll \text{rank}(\mathbf{\Sigma}), \quad (7)$$

and that the K non-zero eigenvalues of \mathbf{S} are all larger than the eigenvalues of $\mathbf{\Sigma}$ and manifest in the K largest eigenvalues of the SCM. Note that the effect of a source will be spread across multiple eigenvalues and eigenvectors if the source is moving and the observation time is not short enough to consider it to be stationary³⁷ or if multiple sources are present and their replica vectors are not orthogonal.³⁸ Hence, a direct correspondence between a particular eigenvalue and a particular loud source might not be possible.

The objective is to separate the components of the SCM $\hat{\mathbf{R}}$ based on its eigenvalues and eigenvectors as

$$\hat{\mathbf{R}} = \sum_{k=1}^K \hat{\lambda}_k \hat{\mathbf{v}}_k \hat{\mathbf{v}}_k^H + \sum_{k=K+1}^N \hat{\lambda}_k \hat{\mathbf{v}}_k \hat{\mathbf{v}}_k^H = \hat{\mathbf{R}}_s + \hat{\mathbf{R}}_n, \quad (8)$$

where $\hat{\mathbf{R}}_s$ is the directional noise component and $\hat{\mathbf{R}}_n$ is the diffuse noise component. The eigenvalues of $\hat{\mathbf{R}}_s$, namely, $\hat{\lambda}_1, \dots, \hat{\lambda}_K$ (and the eigenvectors), also contain a diffuse noise component in addition to the directional noise component and hence the separation of $\hat{\mathbf{R}}$ exactly into $\hat{\mathbf{S}}$ and $\hat{\mathbf{\Sigma}}$ is not possible.

In Sec. II B, we review the case when $\mathbf{R} = \mathbf{R}_n = \mathbf{\Sigma}$, and the true noise CM $\mathbf{\Sigma}$ is due to a spatially isotropic noise field.

B. Relevant results for spatially isotropic noise fields

An isotropic noise field consists of random waves propagating toward the array from all directions. The spatial coherence function of the noise recorded on two sensors in a 3D isotropic noise field is^{39,40}

$$\Gamma = \text{sinc}(2\beta), \quad (9)$$

where $\text{sinc}(x) = \sin(\pi x)/(\pi x)$ and β is the ratio of the spacing between the sensors to the wavelength under consideration ($\beta = fd/c$, where f is the frequency, d is the spacing between the sensors, and c is the speed of wave propagation in the medium). For a linear array of N equidistant sensors, the elements of the CM of the noise field (normalized to unit power on each sensor) are given by

$$\Sigma_{ij} = \text{sinc}(2\beta|i-j|), \quad (10)$$

which is a symmetric Toeplitz matrix. Thus, the spatial correlations are only dependent on β (or equivalently, on f) and the separation $|i-j|$.

1. Asymptotic eigenvalues of the isotropic noise CM

It has been shown that the eigenvalues of an infinite dimensional Toeplitz matrix constructed from sequences in ℓ_1 (absolutely summable), with a Fourier series also in ℓ_1 (called Wiener class Toeplitz matrices) are related to the said Fourier series.⁴¹ Although the sinc sequence is not absolutely summable, the result still holds²³ and the asymptotic eigenvalues of Σ_∞ from Eq. (10) were derived for all β .

In Ref. 23 it is shown that there are at most two distinct eigenvalues (with multiplicities) for all β , given by

$$\Lambda_1 = \frac{q+1}{2\beta} \quad \text{and} \quad \Lambda_2 = \frac{q}{2\beta}, \quad (11)$$

with $q \in \{0, 1, \dots\}$ such that $q < 2\beta \leq q+1$, and the respective multiplicity ratios are given by

$$\xi_1 = 2\beta - q \quad \text{and} \quad \xi_2 = q + 1 - 2\beta. \quad (12)$$

A key result here is the fact that the CM is rank deficient for $\beta < 1/2$, even when $M > N$ because $\Lambda_2 = 0$. In other words, the rank deficiency is not due to insufficient snapshots but due to the nature of the noise field.

2. Asymptotic eigenvalue density of the isotropic noise SCM

The isotropic noise SCM $\hat{\Sigma}$ is modeled as

$$\hat{\Sigma} = \frac{1}{M} \mathbf{X} \mathbf{X}^H, \quad (13)$$

where \mathbf{X} is an $N \times M$ random matrix whose entries are zero-mean complex Gaussian random variables drawn from $\mathcal{CN}(0, 1)$ [Eq. (13) can be verified by taking an expectation]. The probability density of the eigenvalues of $\hat{\Sigma}_\infty$ were derived²³ using Stieltjes transforms³⁶ for $N/M = \nu \leq 1$, i.e., the number of observations (snapshots) is larger than the dimensions of Σ (number of hydrophones).

When the ratio of spacing to wavelength $\beta < 1/2$ or β is a multiple of $1/2$, i.e., $\beta = q/2$, $q \in \mathbb{N}$, the SCM eigenvalue density is given by

$$p_{\hat{\Sigma}_\infty}(\lambda) = \begin{cases} \xi_1 \frac{\sqrt{(\lambda_+ - \lambda)(\lambda - \lambda_-)}}{2\pi\nu\lambda} & \lambda_- < \lambda < \lambda_+ \\ \xi_2 \delta(\lambda) & \text{otherwise,} \end{cases} \quad (14)$$

where $\lambda_\pm = (\sqrt{\Lambda_1} \pm \sqrt{\nu})^2$ are the upper and lower limits of the ‘‘spreading’’ of the eigenvalues of the SCM around the true eigenvalue which is Λ_1 . The density when β is a multiple of $1/2$ is known as the Marčenko–Pastur density.⁴² Regardless of the value of ν , $\hat{\Sigma}$ is rank deficient for all $\beta < 1/2$, as $\xi_2 \neq 0$.

The eigenvalue density of the SCM and the extent of spreading of the eigenvalues for all other values of β can be found in Ref. 23.

III. SEQUENTIAL HYPOTHESIS TESTING OF THE SCM EIGENVALUES

Eigenvalue based sequential testing using RMT was introduced in Ref. 17 for signals in white noise and extended to colored noise in Ref. 22. If the noise only CM is known exactly (or if a noise only SCM can be estimated) and if it can be inverted, one could perform a ‘‘noise whitening’’ transformation²² on the data to transform the underlying noise CM to the identity matrix, following which the eigenvalues can be tested using known results from RMT. However, this is not possible here, as the isotropic noise CM and SCM are inherently rank deficient for $\beta < 1/2$ and hence not invertible. In this section, we outline an approach based on Ref. 17 to distinguish those eigenvalues of the data SCM $\hat{\mathbf{R}}$ that are due to loud sources, from those due to diffuse noise.

Since the number of large eigenvalues K that are dominated by loud sources is not known *a priori*, at each f (or equivalently β), we test sequentially the eigenvalues of $\hat{\mathbf{R}}$, $\{\hat{\lambda}_1, \dots, \hat{\lambda}_N\}$ at each step k (starting with $k=1$) against the following two hypotheses \mathcal{H}_0 (null) and \mathcal{H}_1 (alternate) at a significance level α per test

\mathcal{H}_0 : The k th eigenvalue is due to diffuse noise

\mathcal{H}_1 : The k th eigenvalue is dominated by loud sources, (15)

until \mathcal{H}_0 no longer can be rejected. The termination criterion follows from the fact that the eigenvalues dominated by loud sources are larger than the eigenvalues due to noise only (by definition) and hence once \mathcal{H}_0 cannot be rejected for some k , the subsequent $N - k$ eigenvalues must also be due to diffuse noise.

A. Behavior of the largest eigenvalue of the SCM

1. In a noise only scenario

If there were no loud sources ($K=0$) in the environment and the diffuse noise field is isotropic, the eigenvalues of $\hat{\mathbf{R}} = \hat{\Sigma}$ in the asymptotic limit are distributed as $P_{\hat{\Sigma}_\infty}(\lambda)$. Since no eigenvalues exist⁴³ outside the support of the density $p_{\hat{\Sigma}_\infty}(\lambda)$, the largest eigenvalue of $\hat{\mathbf{R}}_N$, $\hat{\lambda}_1$, converges almost surely to the upper bound of the density,²² λ_+ as $N \rightarrow \infty$.

Typically, the distribution of the largest eigenvalue of complex Wishart matrices is described using the Tracy–Widom (TW) distribution.⁴⁴ For the case when $\mathbf{R} = \mathbf{I}$, the identity matrix, it was shown that the statistic^{17,45}

$$M^{2/3} \frac{\hat{\lambda}_1 - m_{\text{TW}}}{s_{\text{TW}}} \sim \text{TW}, \quad (16)$$

for some scaling constant s_{TW} and centering constant m_{TW} , both dependent on N and M . While these constants can be computed explicitly in this case, it is not straightforward for arbitrary SCMs.⁴⁶

When $\hat{\mathbf{R}} = \hat{\Sigma}$ (diffuse noise only), the equivalent of Eq. (16) can be written as

$$\hat{\lambda}_1 \sim P_{1|\hat{\Sigma}}, \quad (17)$$

where $P_{1|\hat{\Sigma}}(\lambda)$ is the ECD of the largest eigenvalue of $\hat{\Sigma}$. $P_{1|\hat{\Sigma}}(\lambda)$ can be computed in a straightforward fashion from Monte Carlo simulations, as is done in Sec. III B 2.

2. In the presence of loud sources

The presence of loud sources in the environment which are captured in the $K > 0$ large eigenvalues of \mathbf{S} [Sec. II A, under Eq. (6)] manifests in the K largest eigenvalues of the SCM $\hat{\mathbf{R}}$ that are now larger than what they would have been had there been no sources. The eigenvalues of $\hat{\mathbf{R}}$ that are dominated by loud sources are distinguishable from the eigenvalues due to noise when they cross a certain threshold^{22,47} (which depends on the separation between the eigenvalues of \mathbf{S} and Σ , their distributions, and ν). The exact value of the threshold is not relevant to this discussion and here we assume that all the $K \ll \text{rank}(\Sigma)$ largest eigenvalues are distinguishable (although this is not always the case—see the last paragraph of Sec. IV D 1).

The distribution of the K largest eigenvalues in this case is Gaussian^{46,47} (i.e., different from the noise only case) and they can be identified in a statistical hypothesis test [Eq. (15)]. For example, when $K = 1$, the null hypothesis that $\hat{\lambda}_1$ belongs to $P_{1|\hat{\Sigma}}$ [Eq. (15) with $k = 1$] will be rejected with a high probability, indicating that $\hat{\lambda}_1$ is an eigenvalue dominated by loud sources.

B. Inferring the noise eigenvalues

More generally, at step k in the hypothesis test (see Sec. III B 2 for further details), $\hat{\lambda}_k$ (which can be considered to be the largest eigenvalue of an $N - k + 1$ dimensional SCM) is checked to see if it belongs to $P_{1|\hat{\Sigma}_{N-k+1}}$, i.e., the ECD of the largest eigenvalue for an $N - k + 1$ dimensional noise SCM.

The choice of $P_{1|\hat{\Sigma}_{N-k+1}}$ to test $\hat{\lambda}_k$ instead of the more intuitive $P_{k|\hat{\Sigma}}$, i.e., the ECD of the k th eigenvalue of Σ , can be understood from the interlacing properties of eigenvalues (see the Appendix). As a result of Eq. (A1), with $r = k - 1$, $\mathbf{A} = \hat{\Sigma}$, and $\mathbf{A}' = \hat{\Sigma}_{N-k+1}$, the corresponding ECD $P_{k|\hat{\Sigma}}$ is stochastically smaller than $P_{1|\hat{\Sigma}_{N-k+1}}$. Hence, testing $\hat{\lambda}_k$ using $P_{1|\hat{\Sigma}_{N-k+1}}$ provides a conservative p -value for \mathcal{H}_0 (i.e., the actual probability of observing an outlier when \mathcal{H}_0 has not been rejected, is smaller).¹⁷

1. Test statistic

To test $\hat{\lambda}_k$, the test statistic

$$\tau(k) = \frac{\hat{\lambda}_k}{\hat{\sigma}_k^2}, \quad (18)$$

is used, following Ref. 17, with

$$\hat{\sigma}_k^2 = \frac{\bar{\Lambda}}{N' - k + 1} \sum_{i=k}^{N'} \hat{\lambda}_i. \quad (19)$$

Here N' is the number of eigenvalues that are theoretically non-zero and $\bar{\Lambda}$ is the theoretical mean of the N' eigenvalues [see Eq. (20)]. Hence, $\hat{\sigma}^2(k)$ is merely a normalization factor such that the eigenvalues from data can be tested using distributions obtained from simulations.

When $\beta < 1/2$, the noise SCM $\hat{\Sigma}$ is rank deficient because $\xi_2 > 0$ and the corresponding eigenvalues asymptotically are zero (Sec. II B 2). However, in practice they are not *exactly* zero, likely due to sensor noise (self-noise due to system electronics that is independent from element to element). It was observed empirically that including these eigenvalues in the sequential testing often resulted in \mathcal{H}_0 being rejected with a greater likelihood, i.e., eigenvalues that were due to the diffuse noise field were identified incorrectly as being dominated by loud sources (also see Sec. IV B 1).

To avoid this problem, an *ad hoc* correction is made by considering only the largest $N' = \lfloor \xi_1 N \rfloor$ eigenvalues (i.e., only those eigenvalues that theoretically are non-zero) for the sequential testing and accordingly, $\bar{\Lambda} = \Lambda_1$. For all other values of β , $\bar{\Lambda} = 1$ and $N' = N$. In short

$$\bar{\Lambda}, N' = \begin{cases} \Lambda_1, \lfloor \xi_1 N \rfloor & \beta < 1/2 \\ 1, N & \text{otherwise.} \end{cases} \quad (20)$$

2. Hypothesis testing

Starting with $k = 1$, the null hypothesis \mathcal{H}_0 in Eq. (15) is tested at a significance level α and is rejected if

$$\tau(k) > P_{1|\hat{\Sigma}_{N-k+1}}^{-1}(1 - \alpha). \quad (21)$$

The test in Eq. (21) is repeated, incrementing k each time, until \mathcal{H}_0 cannot be rejected. From the resulting value of k , the number of eigenvalues K' that *effectively* are identified as the outliers that are dominated by loud sources, is given by $K' = k - 1$ (see Fig. 1). The remaining $N - K'$ eigenvalues then are considered to be due to diffuse noise. Note that the α here is per test, and not the overall α for the procedure, which is expected to be higher (this typically is controlled using methods such as the Bonferroni correction).

A pre-computed lookup table is generated for $P_{1|\hat{\Sigma}_{N-k+1}}^{-1}(1 - \alpha)$ from 1000 Monte Carlo trials for the given array configuration, for all k and β , assuming a sound speed of $c = 1500$ m/s. One could also perform a simple binary test using the asymptotic upper bounds for the eigenvalue density and get equally good results.²⁶

IV. EXPERIMENTAL RESULTS

A. Data processing

Ocean acoustic data from a bottom mounted horizontal line array (Shark array deployed by the Woods Hole Oceanographic Institution), at a water depth of 79 m with an inter-element spacing of $d = 15$ m are used here. The data were recorded from 13:00:00 to 15:14:24 UTC on

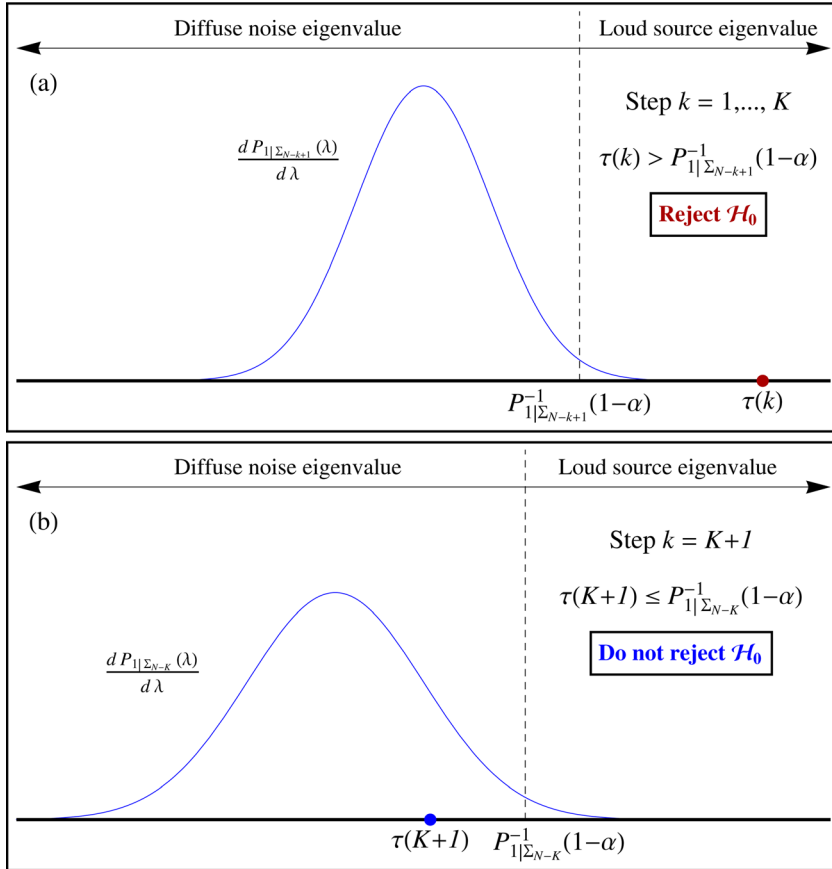


FIG. 1. (Color online) Schematic illustrating the hypothesis test to identify eigenvalues dominated by loud sources. (a) In the presence of K loud sources, the test statistic $\tau(k)$ ($k = \{1, \dots, K\}$) does not belong to the $P_{1|\Sigma_{N-k}}$ distribution when tested at significance α and \mathcal{H}_0 is rejected. (b) The largest eigenvalue from diffuse noise falls inside $P_{1|\Sigma_{N-k+1}}$ and hence \mathcal{H}_0 cannot be rejected.

September 1, 2006 (one day before tropical storm Ernesto) as part of the Office of Naval Research sponsored Shallow Water 2006 experiment conducted off the coast of New Jersey.⁴⁸ Only the data from the first $N = 30$ hydrophones of the 32 element array are used because the 31st hydrophone had inconsistencies in the data.⁹ This dataset was chosen specifically from a time interval where several ships were present in the environment in order to highlight the advantage of this approach where conventional methods do not yield good results.

The data from each hydrophone were bandpass filtered to 20 to 100 Hz and downsampled to a sampling frequency of $f_s = 244.1406$ Hz (500 000 samples every 2048 s). The filtered data were stored in blocks of 128 s each. Each block was further divided into $M = 125$ segments of 1.024 s each and Fourier transformed with a 512 point fast Fourier transform. At each frequency f , the transformed data are written as a column vector $x = [x_1, \dots, x_N]^T$ and the SCM for the block, $\hat{\mathbf{R}}$ is formed as in Eq. (1), with $N = 30$ and $M = 125$.

B. Eigen-structure of the ocean noise field

1. Eigenvalues of the SCM $\hat{\mathbf{R}}$

The sequential hypothesis testing algorithm (Table I) with a significance level $\alpha = 0.05$ is used to separate $\hat{\mathbf{R}}$ into $\hat{\mathbf{R}}_s$ and $\hat{\mathbf{R}}_n$ for each data block at each frequency bin. Visualizing the eigenvalues at a single time slice (128 s from 14:31:44) reveals a rich variation across the frequency [Fig. 2(a)] and the algorithm picks out the outlier eigenvalues quite well at all frequencies (solid line).

The dark triangle to the lower right is the region with zero eigenvalues (theoretically) and corresponds to invisible space.⁴⁹ This is also observed in Fig. 2(b) where the eigenvalues drop past the 16th eigenvalue, which closely corresponds to $\lfloor \xi_1 N \rfloor$ as predicted by theory.¹²

If the correction in Eq. (20) were not applied, it was observed in nearly all the cases that for $\beta < 1/2$ \mathcal{H}_0 was rejected up until about the $(\lfloor \xi_1 N \rfloor + 1)$ th eigenvalue. In other words, only those eigenvalues that theoretically are zero [\times in Fig. 3(b)] were being retained, which was incorrect. Hence, not considering these small eigenvalues results in a better separation of the loud source dominated eigenvalues from the diffuse noise eigenvalues, as can be verified visually in Fig. 3.

TABLE I. Sequential hypothesis testing algorithm.

| Input | |
|---------|---|
| 1. | Frequency f , significance level α , eigenvalues of $\hat{\mathbf{R}}(f), \{\hat{\lambda}_1(f), \dots, \hat{\lambda}_N(f)\}$ |
| 2. | Pre-computed lookup table of $P_{1 \Sigma_{N-k+1}}^{-1}(1-\alpha)$ for $K = \{1, \dots, N\}$ at f |
| Testing | |
| 1. | Assume sound speed, $c = 1500$ m/s |
| 2. | $\beta \leftarrow d/c$ where d is inter-element spacing |
| 3. | Define $\tau(k)$, $\hat{\sigma}_k^2$, and N' as per Eqs. (18)–(20). |
| 4. | $k \leftarrow 1$ |
| 5. | While $\tau(k) > P_{1 \Sigma_{N-k+1}}^{-1}(1-\alpha)$ |
| | Reject \mathcal{H}_0 [see Eq. (15)] |
| | If $k \neq N'$ |
| | $k \leftarrow k + 1$ |
| | Else Break |
| 6. | Return $K' \leftarrow k - 1$ |

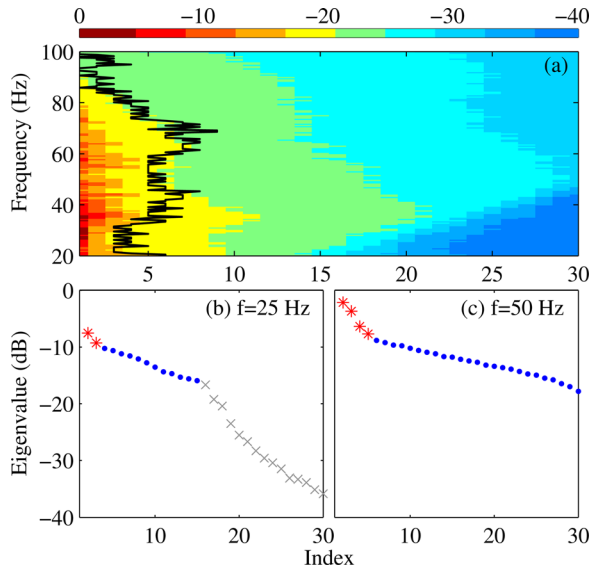


FIG. 2. (Color online) (a) Eigenvalues of the data SCM $\hat{\mathbf{R}}$ (dB) for 20 to 100 Hz at a single time slice. The solid line shows the threshold separating the directional noise (to the left) from the diffuse noise. (b) and (c) Individual eigenvalues at 25 and 50 Hz due to loud sources (*), diffuse noise (\bullet), and eigenvalues not considered [\times , only in (b)]. In each panel, the eigenvalues are normalized by the maximum in that panel.

2. Empirical eigenvalue density

The histogram of the non-zero eigenvalues of $\hat{\mathbf{R}}_n$ from each 128 s realization for the entire 136.5 min duration (normalized to unit mean at each time slice) is shown in

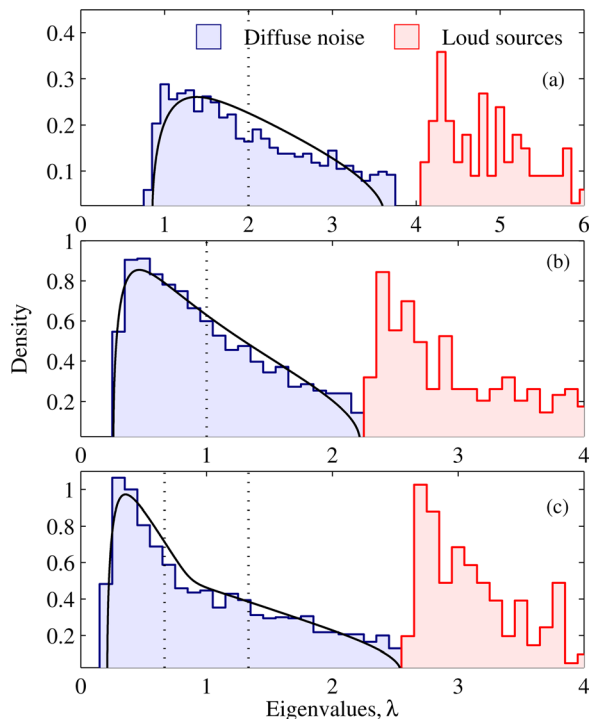


FIG. 3. (Color online) Empirical eigenvalue density (histogram) of the eigenvalues of $\hat{\mathbf{R}}_n$ (under the solid lines) and $\hat{\mathbf{R}}_s$ (to the right) obtained from ocean acoustic data for $f =$ (a) 25, (b) 50, and (c) 75 Hz. The solid lines correspond to the asymptotic eigenvalue density. In (a), only the contribution from the largest $\lceil \xi_1 N \rceil$ eigenvalues are shown. The dotted line(s) show the location(s) of the non-zero eigenvalue(s) of the isotropic noise CM. The densities for the eigenvalues of $\hat{\mathbf{R}}_s$ extend beyond the extent of the panels and is truncated for clarity.

Figs. 3(a)–3(c) for $f = 25, 50,$ and 75 Hz, respectively. Note that since the ensemble of eigenvalues forming the histogram was obtained by discarding a different number of loud source dominated eigenvalues at each realization [on average, 3 to 6 eigenvalues are identified as loud source related for the frequencies shown here; see Fig. 2(a)], the densities shown are not the true densities and Fig. 3 should only be interpreted qualitatively.

Nevertheless, the eigenvalue densities from the data resemble the asymptotic densities (thick solid line) in Sec. II B remarkably well. The histograms of the directional source eigenvalues (from $\hat{\mathbf{R}}_s$ with the same normalization as for $\hat{\mathbf{R}}_n$) are displayed to the right of the corresponding noise eigenvalue densities.

C. Beamformer output

Conventional beamforming with Hamming spatial shading was performed for each block for $\hat{\mathbf{R}}_s$ and $\hat{\mathbf{R}}_n$ at 25 and 50 Hz as

$$B_{(\cdot)}(\theta) = \mathbf{w}^H(\theta) \hat{\mathbf{R}}_{(\cdot)} \mathbf{w}(\theta), \quad (22)$$

where $\mathbf{w}(\theta)$ is the shaded steering vector, with the phase of the n th element given by $w_n(\theta) = \exp[i2\pi f n d / c \sin(\theta)]$, $n = \{0, 1, \dots, N-1\}$.

The dataset shows the presence of a few loud sources in the environment, with two prominent ones being an almost stationary source at about -6° and a source moving from -30° to -80° over the entire duration [“A” and “B,” respectively, in Figs. 4(b) and 4(e)]. The biasing effect of these loud sources in the medium is demonstrated in Sec. IV D 1.

Beamforming on the diffuse noise component demonstrates the isotropic nature of the noise field with nulls only at directions corresponding to the large eigenvalues that were removed [Figs. 4(c) and 4(f)]. The nature of the noise field when the large eigenvalues are re-weighted instead of being removed is discussed in Sec. IV E.

D. Cross-correlations of diffuse noise

1. Convergence of the cross-correlations

The SCM from each subsequent data block is added to the previous, and the resulting averaged cross-correlation is obtained using Eq. (2) as $\langle \hat{C}_{ij}(t) \rangle_T = \mathcal{F}^{-1}[\langle \hat{\mathbf{R}}_{ij}(f) \rangle_T]$, where T denotes the total averaging time. The array configuration (number of hydrophones N and inter-element spacing d), bandwidth, and the choice of observation time M influence the duration of a single block (here 128 s).

Figure 5(d) shows the noise cross-correlations obtained by averaging 64 consecutive instances of $\hat{\mathbf{R}}$ (128 s each) or a total of 136.5 min [evolution of the cross-correlation with successive quadrupling of averaging time in Figs. 5(a)–5(d)]. The dashed lines indicate the predicted travel times for the direct and surface reflected paths, predicted assuming a straight line propagation path, using sound speed measurements in the vicinity of the site (CTD Knorr185-36). The travel times observed can be linked to the location of the directional sources in Figs. 4(b) and 4(e). As the direction of the moving

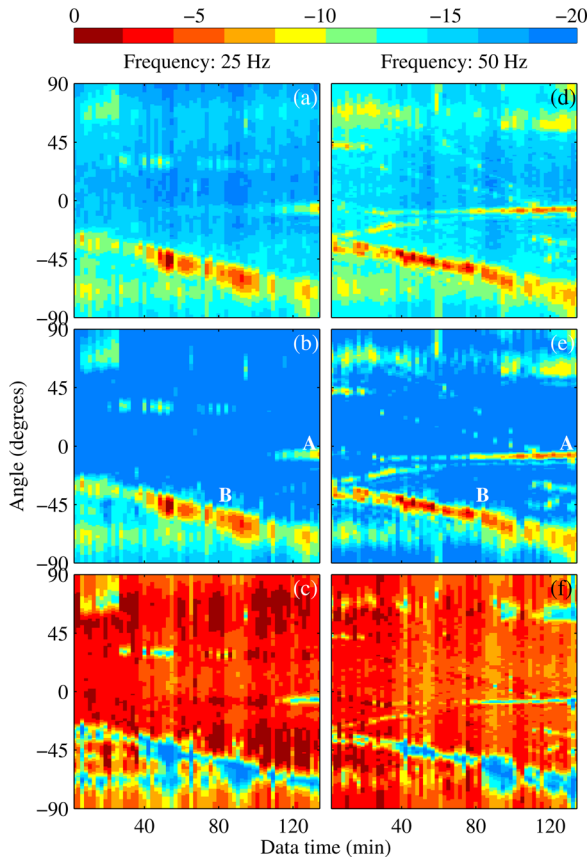


FIG. 4. (Color online) Conventional beamformer output (dB) at 25 and 50 Hz using (a) and (d) $\hat{\mathbf{R}}$, (b) and (e) $\hat{\mathbf{R}}_s$, and (c) and (f) $\hat{\mathbf{R}}_n$. The beamformer output in each panel is normalized by the maximum in that figure. A and B mark the tracks from loud sources.

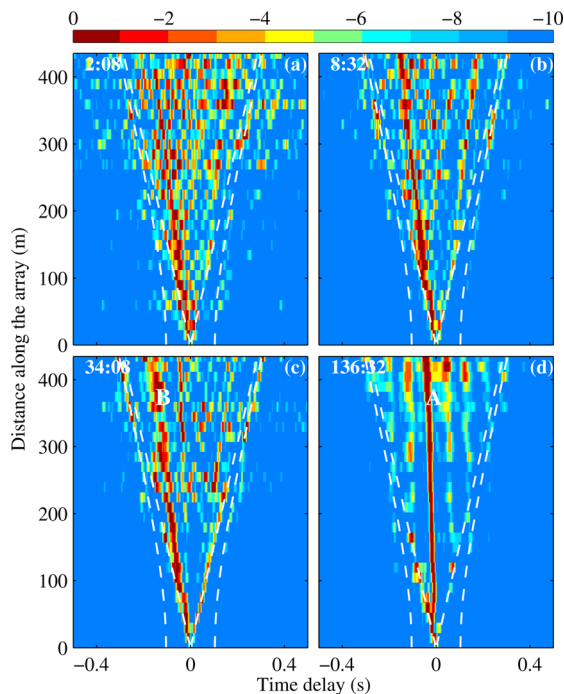


FIG. 5. (Color online) Noise cross-correlations (dB) using $\hat{\mathbf{R}}$. The dashed lines indicate the predicted travel times for the direct (inner) and the surface reflected (outer) paths. Panels (a)–(d) show the evolution of the cross-correlation function with successive quadrupling of averaging time, starting with 2 min in (a). Travel times marked A in (d) and B in (c) correspond to the respective loud sources indicated in Figs. 4(b) and 4(e).

source changes from -30° at the start to -80° at the end of the data window [B in Figs. 4(b) and 4(e)], the corresponding travel time also changes accordingly [B in Fig. 5(d)]. Slowly moving sources build up correlation peaks steadily and dominate the observed travel times [A in Fig. 5(d)]. These figures illustrate the effect of directional noise sources in the medium, which results in several spurious arrivals that are visible at correlation times less than the predicted times and reduce the reliability of the travel time estimates.

In contrast, the noise cross-correlations obtained using $\hat{\mathbf{R}}_n$ instead of $\hat{\mathbf{R}}$ (as before, averages of 64 consecutive instances) in Eq. (2) have a two-sided (symmetric) structure (Fig. 6). A two-sided cross-correlation is typical for a diffuse noise field, and the negative time delays correspond to a propagation direction opposite that of the positive time delays. The observed travel times also correspond well to the predicted travel times (see Fig. 7). A faster arrival with a symmetric component is observed [C in Fig. 6(d)], which could possibly correspond to a propagation path through the sediment layer.

One also sees a weak arrival close to zero lag [A in Fig. 6(d)], which is due to residual components from the loud source at -6° [A in Figs. 4(b) and 4(e)] that the eigenvalue processing failed to remove. A likely reason is that this source was not loud enough to be detected by the algorithm (see discussion in Sec. III A 2). Yet, it built up a correlation peak because it was moving slowly.

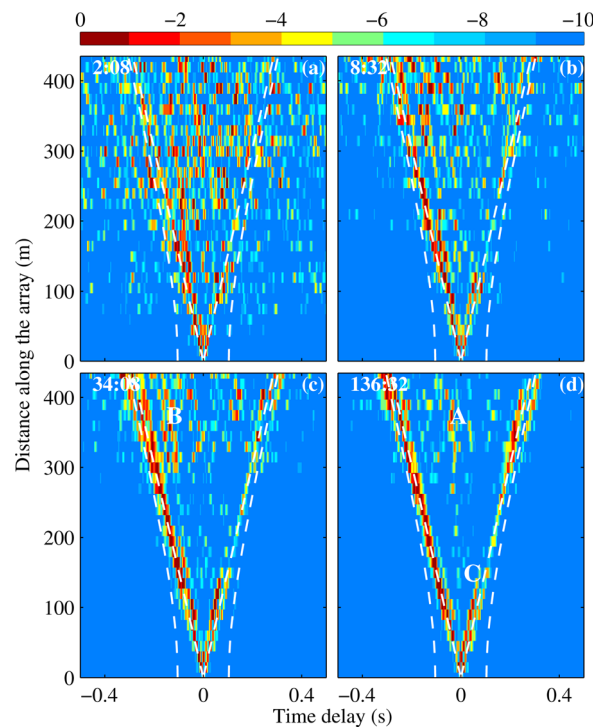


FIG. 6. (Color online) Noise cross-correlations (dB) using $\hat{\mathbf{R}}_n$. Dashed lines indicate the predicted travel times for the direct (inner) and the surface reflected (outer) paths. Panels (a)–(d) show the evolution of the cross-correlation function with successive quadrupling of averaging time starting with 2 min in (a). Travel time marked A in (d) and B in (c) correspond to the respective loud sources indicated in Figs. 4(b) and 4(e). C marks an arrival (which has a symmetric component) that could possibly correspond to a propagation path through the bottom layer.

2. SNR

The signal-to-noise ratio (SNR) of the cross-correlation buildup is also studied as a function of averaging time for the data considered here. Here, SNR is defined as the ratio of the maximum of the cross-correlation in a 0.025 s window around the predicted travel time to the standard deviation of the fluctuations at large correlation times [see trace at 240 m in Figs. 8(a) and 8(b), same trace also shown on top of Fig. 7].⁷ This definition helps track the buildup of the SNR at the predicted time, and avoids skewing of the result due to the peak in the data being shifted due to directional sources.

When there are loud sources in the environment that are in motion, the location of the correlation peaks vary with the direction of the source and hence the SNR does not build up steadily and fluctuates with time [see Fig. 8(c)]. On the other hand, when the loud sources are removed, the peaks build up along the travel times corresponding to propagation along the end-fire direction and the SNR shows a steady increase, proceeding as the square-root of averaging time T as predicted by theory (dashed line).⁷

E. Cross-correlations from re-weighted eigenvalues

Although the cross-correlations obtained using $\hat{\mathbf{R}}_n$ provide reliable results (Sec. IV D), it does not utilize the entire diffuse noise field because the separated diffuse noise component has spatial voids in directions corresponding to the large eigenvalues that were removed [Figs. 4(c) and 4(f)]. This is because the eigenvalues and eigenvectors of $\hat{\mathbf{R}}_s$ also include contributions from the diffuse noise field (Sec. II A) which cannot be separated. Since the biasing effect in cross-correlations is caused by the non-zero eigenvalues of $\hat{\mathbf{R}}_s$, it is also possible to mitigate their effect by re-weighting the large eigenvalues instead of removing them entirely.

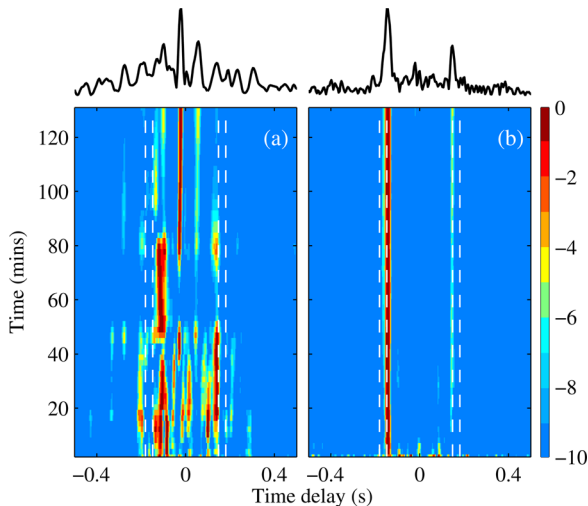


FIG. 7. (Color online) Averaged cross-correlations between sensors 1 and 16 (spaced 240 m apart) obtained using (a) $\hat{\mathbf{R}}$ and (b) $\hat{\mathbf{R}}_n$ with increasing averaging time. The maximum in each trace has been normalized to 1 for plotting purposes in order to highlight the peaks. The result after averaging or 136.5 min (solid line) is shown above the respective plots. Dashed lines indicate the predicted travel times for the direct (inner) and the surface reflected (outer) paths.

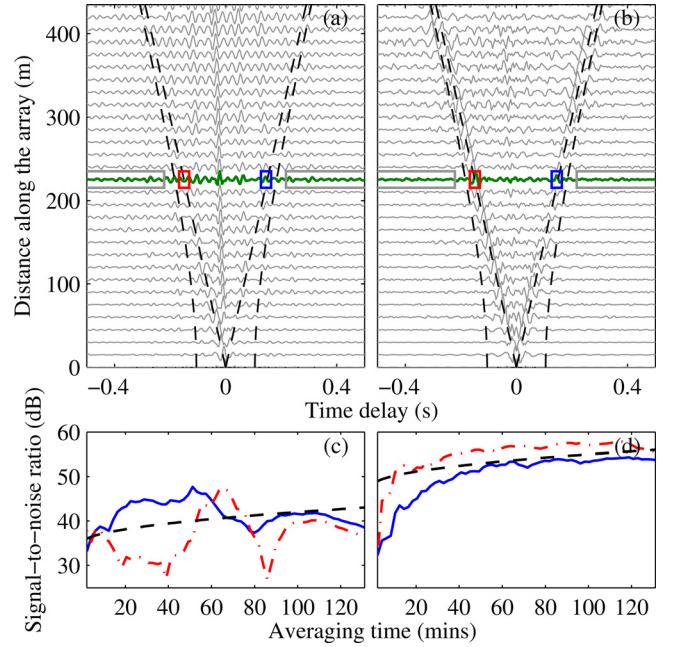


FIG. 8. (Color online) (a) and (b) Noise cross correlations using the data SCM $\hat{\mathbf{R}}$ and the diffuse noise SCM $\hat{\mathbf{R}}_n$, respectively, after 136.5 min of averaging. (c) and (d) SNR for the positive (solid line) and negative (dotted-dashed line) time delay of the noise cross-correlation function between sensors 1 and 16 [highlighted in (a) and (b)] with increasing averaging time using $\hat{\mathbf{R}}$ and $\hat{\mathbf{R}}_n$, respectively. The dashed line shows the square root of the time curve, which is the SNR build up predicted by theory.

Consider a re-synthesized SCM $\tilde{\mathbf{R}}$ obtained as

$$\tilde{\mathbf{R}} = \sum_{k=1}^{K'} \tilde{\lambda}_k \hat{\mathbf{v}}_k \hat{\mathbf{v}}_k^H + \hat{\mathbf{R}}_n, \quad (23)$$

where $\tilde{\lambda}_k$ are the re-weighted eigenvalues ($\tilde{\lambda} = 0$ in Sec. IV D). There are several ways in which the weights can be assigned, and two straightforward weightings are considered here.

1. $\tilde{\lambda}_i = \text{Mean of the noise eigenvalues, i.e.,}$

$$\tilde{\lambda}_i = \frac{1}{N' - K'} \sum_{k=K'+1}^{N'} \hat{\lambda}_k, \quad i = 1, \dots, K'. \quad (24)$$

2. $\tilde{\lambda}_i = \text{Largest noise eigenvalue, i.e.,}$

$$\tilde{\lambda}_i = \hat{\lambda}_{K'+1}, \quad i = 1, \dots, K'. \quad (25)$$

In both cases, the resulting noise field [Figs. 9(a) and 9(b)] does not exhibit the spatial voids observed when using only $\hat{\mathbf{R}}_n$ [Figs. 4(c) and 4(f)]. The 136.5 min averaged cross-correlations using $\tilde{\mathbf{R}}$ with the weights in Eq. (24) [Fig. 9(c)], are very similar to that obtained using $\hat{\mathbf{R}}_n$ [Fig. 6(d)]. However, using the weights in Eq. (25) gives a cross-correlation structure that has both the arrivals at the predicted travel times and a spurious arrival [A in Fig. 9(d)] corresponding to the slowly moving source at -6° [A in Figs. 4(b) and 4(e)]. This spurious arrival can easily be discarded by time-gating. The surface-reflected arrival is also visible from 150 m in range onwards [D in Fig. 9(d)], whereas it is only visible

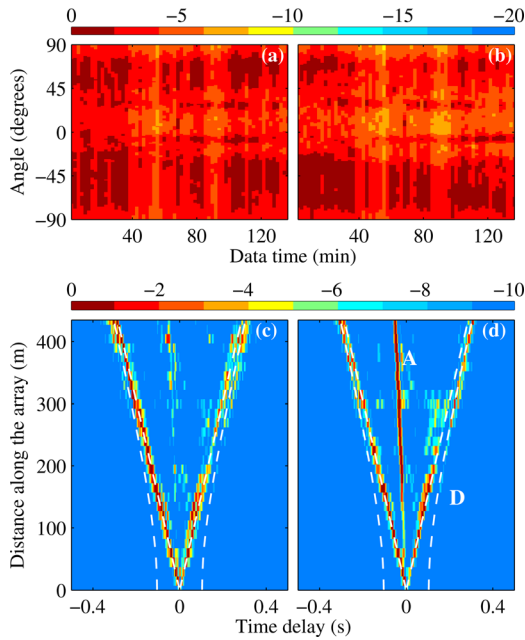


FIG. 9. (Color online) Beamformer outputs (dB) at 25 Hz (a) and (b) and cross-correlations (dB) from 136.5 min of averaging (c) and (d) obtained by re-weighting the large eigenvalues using Eq. (24) in (a) and (c) and Eq. (25) in (b) and (d).

from 300 m onwards in Figs. 6(d) and Fig. 9(c). As seen from the two examples, changing the weights can lead to different results and each approach can be advantageous in different scenarios.

V. IMPACT OF ALTERNATIVE OCEAN DIFFUSE NOISE MODELS

Here we compare qualitatively the impact of using three alternative ocean noise models for the hypothesis testing in addition to the 3D isotropic model (ISO) already considered in this article—surface noise in a fluid half-space (Cron–Sherman model⁵⁰ with omnidirectional sources

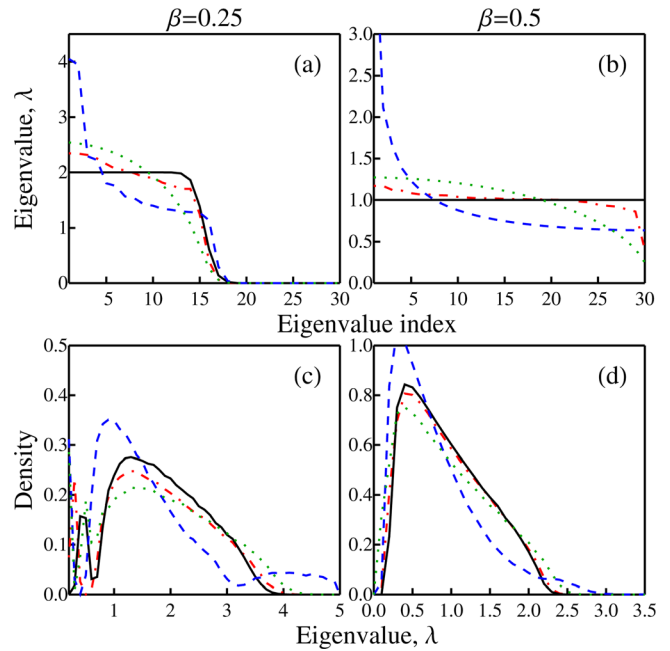


FIG. 10. (Color online) Eigenvalues of the CM for the 3D isotropic noise model (ISO, solid line), the Cron–Sherman model for surface noise in a fluid half-space with omnidirectional sources (CS0, dashed line), and sources with cosine directionality (CS1, dotted line), and the KI model for surface noise in a waveguide with a sediment layer (KI using measured environment parameters, dotted-dashed line) with $N = 30$ hydrophones and $\beta = 0.25$ (a) and $\beta = 0.5$ (b). (c) and (d) Empirical eigenvalue density of the SCMs ($\nu = 30/125$) corresponding to the CMs in (a) and (b) obtained from 1000 Monte Carlo trials.

(CS0) and cosine directional sources (CS1), and surface noise in a waveguide with a sediment layer (Kuperman–Ingenito model,⁵¹ KI). KI is a more complicated noise model that incorporates waveguide physics and is representative of ocean noise in shallow water environments. It is used here primarily to show the similarities between the simpler models (which do not require any knowledge of the environment) and a model based on the local environment.

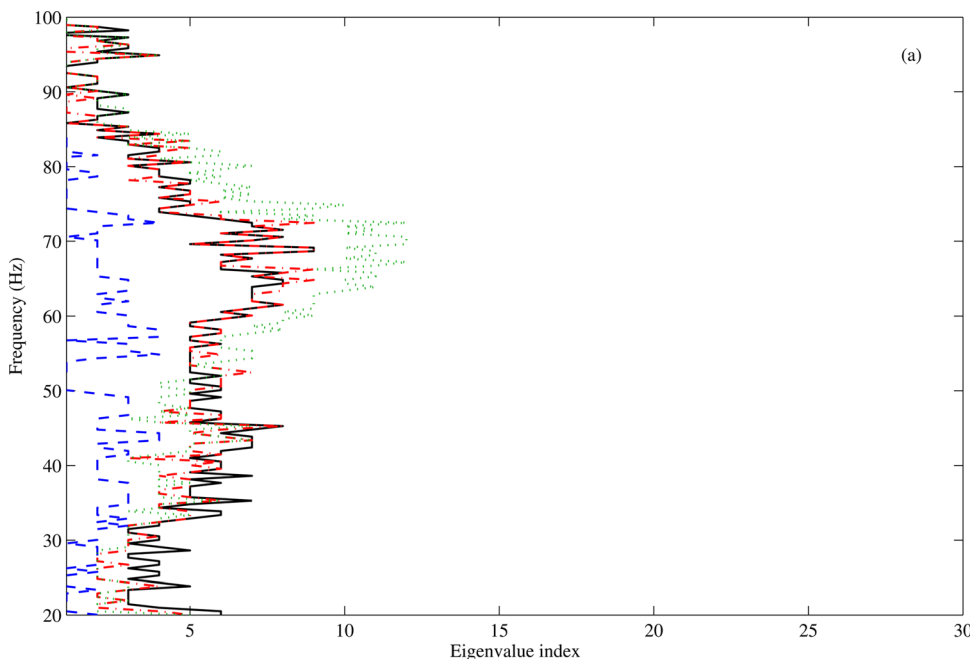


FIG. 11. (Color online) Threshold separating the directional noise (to the left) from the diffuse noise is shown at a single time slice for the 3D isotropic noise model (ISO, solid line), the Cron–Sherman model for surface noise in a fluid half-space due to omnidirectional sources (CS0, dashed line) and cosine directional sources (CS1, dotted line), and the KI model for surface noise in a waveguide with a sediment layer (KI, dotted–dashed line).

The CMs for the noise models using the array configuration in Sec. IV A and a medium sound speed of 1500 m/s are obtained using Eq. (10) for Σ^{ISO} and

$$\Sigma_{ij}^{\text{CS0}} = J_0(2\pi\beta|i-j|), \quad (26)$$

$$\Sigma_{ij}^{\text{CS1}} = \frac{2J_1(2\pi\beta|i-j|)}{2\pi\beta|i-j|}, \quad (27)$$

where J_0 and J_1 are the Bessel functions of the first kind and zeroth and first orders, respectively. The KI model, Σ^{KI} , is generated by a wavenumber integration approach using OASES⁵² assuming a 79 m deep stratified waveguide (using a sound speed profile from CTD measurements at the site) and a seabed with sound speed⁹ 1650 m/s and density 1.69 g/cm³.

Figure 10 shows the eigenvalues of the CM for the different noise models for $\beta=0.25$ (a) and $\beta=0.5$ (b). The eigenvalues of Σ^{ISO} are very close to that of Σ^{KI} (assumed to be true), and those of Σ^{CS1} , while similar in general structure to KI, show more deviation. The CS0 model least resembles KI and shows a large deviation. The small differences between the eigen-structure of Σ^{KI} and those of Σ^{ISO} and Σ^{CS1} are further reduced in their respective SCMs as observed by the similarity in the eigenvalue density (obtained from 1000 Monte Carlo trials) of $\hat{\Sigma}^{\text{KI}}$ to that of $\hat{\Sigma}^{\text{ISO}}$ [Figs. 10(c) and 10(d)]. This is related to the general spreading of eigenvalues observed in SCMs. The similarity in the density holds when the observations $M \sim N$ and decrease as $M \rightarrow \infty$. In contrast, the eigenvalue density of $\hat{\Sigma}^{\text{CS0}}$ remains different from the rest in shape and the upper edge of the density.

Intuitively, one would expect a density with a larger value of $P_{1|\hat{\Sigma}_{N-k+1}^{(\cdot)}}^{-1}(1-\alpha)$ such as that for $\hat{\Sigma}^{\text{CS0}}$ to reject \mathcal{H}_0

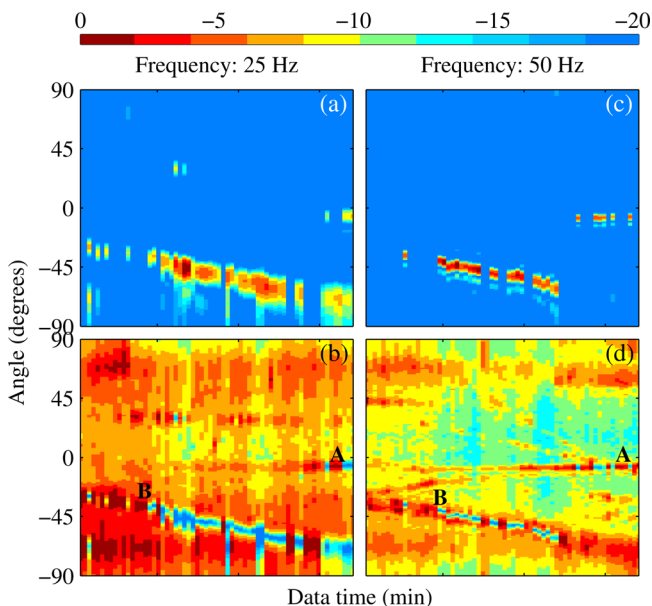


FIG. 12. (Color online) Conventional beamformer output (dB) at 25 and 50 Hz using (a) and (c) $\hat{\mathbf{R}}_s$ and (b) and (d) $\hat{\mathbf{R}}_n$ obtained by using the Cron-Sherman model for surface noise in a fluid half-space due to omnidirectional sources (CS0) for the hypothesis testing. The beamformer output in each panel is normalized by the maximum in that panel.

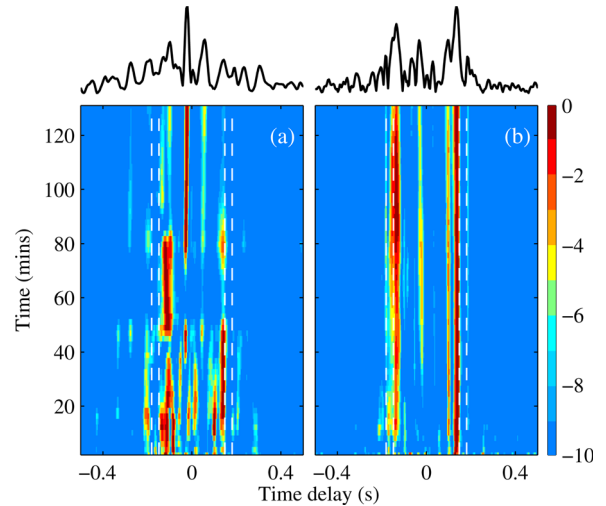


FIG. 13. (Color online) Averaged cross-correlations between sensors 1 and 16 (spaced 240 m apart) obtained using (a) $\hat{\mathbf{R}}$ [same as Fig. 7(a)] and (b) $\hat{\mathbf{R}}_n$ with the hypothesis test performed using the Cron-Sherman model for surface noise in a fluid half-space due to omnidirectional sources (CS0).

less often, i.e., rejecting it only in cases where the loud source eigenvalue is very large (compared to the other models). This is indeed the case, as seen from Fig. 11, where the thresholds separating the loud source subspace and the diffuse noise subspace are shown for the different models. As expected from the similarities in the density, the thresholds obtained using ISO (solid line) are nearly identical to that from KI (dotted-dashed line), differing by at most one or two. CS1 (dotted line) also follows the general pattern for the KI and 3D thresholds. CS0 (dashed line), which showed the most deviation, identifies only the very largest of the loud source eigenvalues.

The effect of a shifted threshold arising from a poorly chosen model is seen clearly in the beamformer output in Fig. 12 using the CS0 model (results for KI and CS1 are very similar to those of ISO shown earlier in Sec. IV and hence are not shown here). Several ship tracks are identifiable in the “diffuse noise” subspace that is obtained using the CS0 model [A and B in Figs. 12(b) and 12(d); compare with Figs. 4(c) and 4(f)] and the resulting noise cross-correlations are still contaminated by spurious arrivals from loud sources [Fig. 13(a)].

In summary, simple analytical noise models which do not require any additional knowledge of the environment can be used as a reasonable approximation to more sophisticated models that incorporate waveguide physics and environmental information for the purposes of eigenvalue based statistical inference.

VI. CONCLUSIONS

In this paper, we have demonstrated an eigenvalue based approach to separate ocean noise into directional and diffuse components. By approximating the diffuse noise recorded on a hydrophone array to be isotropic in nature, the eigenvalues of the data sample covariance (SCM) are analyzed. Insights from RMT are then used to explain the nature of the noise eigenvalues and a sequential hypothesis testing is performed to identify, and isolate or attenuate the loud, directional sources.

The resulting cross-correlations were shown to converge quickly and remain stable with increasing averaging time. The structure of the resulting cross-correlations are two-sided (positive and negative time delays), which reduces the ambiguity in the estimates of the travel time. The SNR of the cross-correlations was also shown to increase as the square root of time, which is consistent with theoretical predictions.

Finally, the impact of the chosen noise model on the identification of loud sources and cross-correlations were analyzed and it was shown that simple analytical noise models provide similar results as more sophisticated noise models that mimic the environment.

ACKNOWLEDGMENTS

This work was supported by the Office of Naval Research, Grant Nos. N00014-11-1-0320 and N00014-11-1-0321.

APPENDIX: INTERLACING OF EIGENVALUES

Let \mathbf{A} be any $N \times N$ Hermitian matrix, with eigenvalues $a_1 \geq a_2 \geq \dots \geq a_N$ and \mathbf{A}' be the $(N-r) \times (N-r)$ Hermitian matrix obtained by removing r rows and the corresponding r columns, with eigenvalues $a'_1 \geq a'_2 \geq \dots \geq a'_{N-r}$. Then, the eigenvalues of \mathbf{A} and \mathbf{A}' interlace as

$$a_i \geq a'_i \geq a_{i+r}, \quad (\text{A1})$$

for $i \in \{1, \dots, N-r\}$. Proof of Eq. (A1) can be found in Ref. 53 (Theorem 4.3.15).

¹O. I. Lobkis and R. L. Weaver, "On the emergence of the Green's function in the correlations of a diffuse field," *J. Acoust. Soc. Am.* **110**, 3011–3017 (2001).
²R. L. Weaver and O. I. Lobkis, "Ultrasonics without a source: Thermal fluctuation correlations at MHz frequencies," *Phys. Rev. Lett.* **87**, 134301 (2001).
³R. Snieder, "Extracting the Green's function from the correlation of coda waves: A derivation based on stationary phase," *Phys. Rev. E* **69**, 046610 (2004).
⁴K. Wapenaar, "Retrieving the elastodynamic Green's function of an arbitrary inhomogeneous medium by cross-correlation," *Phys. Rev. Lett.* **93**, 254301 (2004).
⁵O. A. Godin, "Recovering the acoustic Green's function from ambient noise cross correlation in an inhomogeneous moving medium," *Phys. Rev. Lett.* **97**, 054301 (2006).
⁶P. Roux, W. A. Kuperman, and the NPAL group, "Extracting coherent wave fronts from acoustic ambient noise in the ocean," *J. Acoust. Soc. Am.* **116**, 1995–2003 (2004).
⁷K. G. Sabra, P. Roux, and W. A. Kuperman, "Emergence rate of the time-domain Green's function from the ambient noise cross-correlation," *J. Acoust. Soc. Am.* **118**, 3524–3531 (2005).
⁸M. Siderius, C. H. Harrison, and M. B. Porter, "A passive fathometer technique for imaging seabed layering using ambient noise," *J. Acoust. Soc. Am.* **120**, 1315–1323 (2006).
⁹L. A. Brooks and P. Gerstoft, "Green's function approximation from cross-correlations of 20–100 Hz noise during a tropical storm," *J. Acoust. Soc. Am.* **125**, 723–734 (2009).
¹⁰J. Traer, P. Gerstoft, and W. S. Hodgkiss, "Ocean bottom profiling with ambient noise: A model for the passive fathometer," *J. Acoust. Soc. Am.* **129**, 1825–1836 (2011).
¹¹N. M. Shapiro, M. Campillo, L. Stehly, and M. H. Ritzwoller, "High-resolution surface-wave tomography from ambient seismic noise," *Science* **307**, 1615–1618 (2005).

¹²P. Gerstoft, K. G. Sabra, P. Roux, W. A. Kuperman, and M. C. Fehler, "Green's functions extraction and surface-wave tomography from microseisms in southern California," *Geophysics* **71**, SI23–SI31 (2006).
¹³P. Gouédard, L. Stehly, F. Brenguier, M. Campillo, Y. C. de Verdière, E. Larose, L. Margerin, P. Roux, F. J. Sánchez-Sesma, N. M. Shapiro, and R. L. Weaver, "Cross-correlation of random fields: Mathematical approach and applications," *Geophysical Prospect.* **56**, 375–393 (2008).
¹⁴S. C. Walker and M. J. Buckingham, "Spatial coherence and cross-correlation of three-dimensional ambient noise fields in the ocean," *J. Acoust. Soc. Am.* **131**, 1079–1086 (2012).
¹⁵V. C. Tsai, "On establishing the accuracy of noise tomography travel-time measurements in a realistic medium," *Geophys. J. Int.* **178**, 1555–1564 (2009).
¹⁶M. L. Mehta, *Random Matrices*, 3rd ed. (Academic, New York, 2004), Chap. 1.
¹⁷I. M. Johnstone, "On the distribution of the largest eigenvalue in principal components analysis," *Ann. Stat.* **29**, 295–327 (2001).
¹⁸N. E. Karoui, "Spectrum estimation for large dimensional covariance matrices using random matrix theory," *Ann. Stat.* **36**, 2757–2790 (2008).
¹⁹X. Mestre and M. A. Lagunas, "Finite sample size effect on minimum variance beam-formers: Optimum diagonal loading factor for large arrays," *IEEE Trans. Signal Process.* **54**, 69–82 (2006).
²⁰X. Mestre, "On the asymptotic behaviour of the sample estimates of eigenvalues and eigenvectors of covariance matrices," *IEEE Trans. Signal Process.* **56**, 5353–5368 (2008).
²¹R. R. Nadakuditi and A. Edelman, "Sample eigenvalue based detection of high-dimensional signals in white noise using relatively few samples," *IEEE Trans. Signal Process.* **56**, 2625–2638 (2008).
²²R. R. Nadakuditi and J. W. Silverstein, "Fundamental limit of sample generalized eigenvalue based detection of signals in noise using relatively few signal-bearing and noise-only samples," *IEEE J. Sel. Top. Signal Process.* **4**, 468–480 (2010).
²³R. Menon, P. Gerstoft, and W. S. Hodgkiss, "Asymptotic eigenvalue density of noise covariance matrices," *IEEE Trans. Signal Process.* **60**, 3415–3424 (2012).
²⁴M. Pajovic, J. Preisig, and A. Baggeroer, "Analytical characterization of the mpdr-based power estimators in snapshot scarce regime," *IEEE Stat. Signal Proc. Workshop (Ann Arbor, Michigan)*, pp. 812–815 (2012).
²⁵J. R. Buck and K. Wage, "A random matrix theory model for the dominant mode rejection beamformer notch depth," *IEEE Stat. Signal Proc. Workshop (Ann Arbor, Michigan)*, pp. 824–827 (2012).
²⁶R. Menon, P. Gerstoft, and W. S. Hodgkiss, "Passive acoustic monitoring using random matrix theory," *IEEE Stat. Signal Proc. Workshop (Ann Arbor, Michigan)*, pp. 808–811 (2012).
²⁷P. Gerstoft, R. Menon, W. S. Hodgkiss, and C. F. Mecklenbräuker, "Eigenvalues of the sample covariance matrix for a towed array," *J. Acoust. Soc. Am.* **132**, 2388–2396 (2012).
²⁸K. Wage, J. Buck, M. Dzieciuch, and P. Worcester, "Experimental validation of a random matrix theory model for dominant mode rejection beamformer notch depth," *IEEE Stat. Signal Proc. Workshop (Ann Arbor, Michigan)*, pp. 820–823 (2012).
²⁹S. Tuladhar, J. Buck, and K. Wage, "Approximate eigenvalue distribution of a cylindrically isotropic noise sample covariance matrix," *IEEE Stat. Signal Proc. Workshop (Ann Arbor, Michigan)*, pp. 828–831 (2012).
³⁰R. R. Müller, "A random matrix model of communication via antenna arrays," *IEEE Trans. Inf. Theory* **48**, 2495–2506 (2002).
³¹A. M. Tulino and S. Verdú, "Random matrix theory and wireless communications," *Found. Trends Commun. Inf. Theory* **1**, 1–182 (2004).
³²R. L. Weaver, "Spectral statistics in elastodynamics," *J. Acoust. Soc. Am.* **85**, 1005–1013 (1989).
³³A. Aubry and A. Derode, "Random matrix theory applied to acoustic backscattering and imaging in complex media," *Phys. Rev. Lett.* **102**, 084301 (2009).
³⁴A. Aubry and A. Derode, "Detection and imaging in a random medium: A matrix method to overcome multiple scattering and aberration," *J. Appl. Phys.* **106**, 044903 (2009).
³⁵S. E. Skipetrov and A. Goetschy, "Eigenvalue distributions of large Euclidean random matrices for waves in random media," *J. Phys. A: Math. Theor.* **44**, 065102 (2011).
³⁶J. W. Silverstein, "Strong convergence of the empirical distribution of eigenvalues of large dimensional random matrices," *J. Multivariate Anal.* **54**, 175–192 (1995).

- ³⁷A. B. Baggeroer and H. Cox, "Passive sonar limits upon nulling multiple moving ships with large aperture arrays," in *33rd ASILOMAR Conference on Signals Systems and Computers*, Vol. 1, pp. 103–108 (1999).
- ³⁸D. H. Johnson and D. E. Dudgeon, *Array Processing: Concepts and Techniques* (Prentice Hall, Englewood Cliffs, NJ, 1993), Chap. 7.3.
- ³⁹C. H. Eckart, "The theory of noise in continuous media," *J. Acoust. Soc. Am.* **25**, 195–199 (1953).
- ⁴⁰H. Cox, "Spatial correlation in arbitrary noise fields with application to ambient sea noise," *J. Acoust. Soc. Am.* **54**, 1289–1301 (1973).
- ⁴¹R. M. Gray, "Toeplitz and circulant matrices: A review," *Found. Trends. Comm. Inf. Theory* **2**, 155–239 (2006).
- ⁴²V. A. Marčenko and L. A. Pastur, "Distributions of eigenvalues of some sets of random matrices," *Math. USSR. Sb.* **72**, 507–536 (1967).
- ⁴³Z. Bai and J. W. Silverstein, "No eigenvalues outside the support of the limiting spectral distribution of large dimensional sample covariance matrices," *Ann. Probab.* **26**, 316–345 (1998).
- ⁴⁴C. A. Tracy and H. Widom, "Level-spacing distributions and the Airy kernel," *Commun. Math. Phys.* **159**, 151–174 (1994).
- ⁴⁵K. Johansson, "Shape fluctuations and random matrices," *Commun. Math. Phys.* **209**, 437–476 (2000).
- ⁴⁶N. E. Karoui, "Tracy-Widom limit for the largest eigenvalue of a large class of complex sample covariance matrices," *Ann. Probab.* **35**, 663–714 (2007).
- ⁴⁷J. Baik, G. B. Arous, and S. Pécché, "Phase transition of the largest eigenvalue for nonnull complex sample covariance matrices," *Ann. Probab.* **33**, 1643–1697 (2005).
- ⁴⁸D. J. Tang, J. Moum, J. Lynch, P. Abbot, R. Chapman, P. Dahl, T. Duda, G. Gawarkiewicz, S. Glenn, J. Goff, H. Graber, J. Kemp, A. Maffei, J. Nash, and A. Newhall, "Shallow Water 2006: A joint acoustic propagation/nonlinear internal wave physics experiment," *Oceanogr.* **20**, 156–167 (2007).
- ⁴⁹D. H. Johnson and D. E. Dudgeon, *Array Processing: Concepts and Techniques* (Prentice Hall, Englewood Cliffs, NJ, 1993), Chap. 3.
- ⁵⁰B. F. Cron and C. H. Sherman, "Spatial correlation functions for various noise models," *J. Acoust. Soc. Am.* **34**, 1732–1736 (1962).
- ⁵¹W. A. Kuperman and F. Ingenito, "Spatial correlation of surface generated noise in a stratified ocean," *J. Acoust. Soc. Am.* **67**, 1988–1996 (1980).
- ⁵²H. Schmidt, *OASES Version 3.1 User Guide and Reference Manual* (MIT, Cambridge, MA, 2004), 175 p.
- ⁵³R. A. Horn and C. R. Johnson, *Matrix Analysis* (Cambridge University, Cambridge, 1985), Chap. 4.